Experimental realization of Shor's quantum factoring algorithm using nuclear magnetic resonance

Lieven M.K. Vandersypen[†,*], Matthias Steffen[*,†], Gregory Breyta[†],
Costantino S. Yannoni[†], Mark H. Sherwood[†] and Isaac L. Chuang[*,†]

[†] *IBM Almaden Research Center,*
San Jose, CA 95120
[*] *Solid State and Photonics Laboratory,*
Stanford University,
Stanford, CA 94305-4075

1

The number of steps any classical computer requires in order to find the prime factors of an l-digit integer N increases exponentially with l, at least using algorithms [1] known at present. Factoring large integers is therefore conjectured to be intractable classically, an observation underlying the security of widely used cryptographic codes [1, 2]. Quantum computers [3], however, could factor integers in only polynomial time, using Shor's quantum factoring algorithm [4, 5, 6]. Although important for the study of quantum computers [7], experimental demonstration of this algorithm has proved elusive [8, 9, 10]. Here we report an implementation of the simplest instance of Shor's algorithm: factorization of N=15 (whose prime factors are 3 and 5). We use seven spin-1/2 nuclei in a molecule as quantum bits [11, 12], which can be manipulated with room temperature liquid state nuclear magnetic resonance techniques. This method of using nuclei to store quantum information is in principle scalable to many quantum bit systems [13], but such scalability is not implied by the present work. The significance of our work lies in the demonstration of experimental and theoretical techniques for precise control and modelling of complex quantum computers. In particular, we present a simple, parameter-free but predictive model of decoherence effects [14] in our system.

Shor's factoring algorithm works by utilizing a quantum computer to quickly determine the period of the function $f(x) = a^x \bmod N$ (the remainder of a^x divided by N), where a is a randomly chosen small number with no factors in common with N; from this period, number-theoretic techniques can be employed to factor N with high probability [4]. The two main components of the algorithm, modular exponentiation (computation of $a^x \bmod N$) and the inverse quantum Fourier transform (QFT) take only $\mathcal{O}(l^3)$ operations [4, 5, 6]. Classically, in contrast, prime factorization takes $\mathcal{O}(2^{l^{1/3}})$ operations [1], which quickly becomes intractable as l increases.

The simplest meaningful instance of Shor's algorithm is factorization of $N = 15$ [7] — the algorithm fails for N even or a prime power. Even for such a small N, quantum factorization poses at

present a significant experimental challenge: it requires coherent control over seven quantum bits (qubits) in the course of a long sequence of controlled interactions, even after maximal reduction of the quantum circuit; including the state initialization, interactions between almost all pairs of qubits are needed. In comparison with earlier work [8, 9, 10], this experiment thus puts extraordinarily high demands on the spin-spin coupling network, the degree of control over the Hamiltonian and the spin coherence times. Furthermore, numerically predicting the outcome of these experiments has been considered impractical due to the enormous size of the state space transformations, which are described by $\sim 4^7 \times 4^7$ real parameters if decoherence effects are included.

Implementation of the algorithm can be broken into four distinct steps (Fig. 1a), with the most complex being the computation of $f(x) = a^x \bmod N$ for 2^n values of x in parallel. Following standard classical circuit techniques, this is performed by utilizing the identity $a^x = a^{2^{n-1}x_{n-1}} \ldots a^{2x_1} a^{x_0}$, where x_k are the binary digits of x. Modular exponentiation thus consists of serial multiplication by $a^{2^k} \bmod N$ for all k ($0 \le k \le n-1$) for which $|x_k\rangle = |1\rangle$. The powers a^{2^k} can be efficiently pre-computed on a classical machine by repeated squaring of a. For $N = 15$, a may be $2, 4, 7, 8, 11, 13$ or 14. If we happen to pick $a = 2, 7, 8$ or 13, we find that $a^4 \bmod 15 = 1$, and therefore all $a^{2^k} \bmod N = 1$ for $k \ge 2$. In this case, $f(x)$ simplifies to multiplications controlled by just two bits, x_0 and x_1. If $a = 4, 11$ or 14, then $a^2 \bmod 15 = 1$, so only x_0 is relevant. Thus, the first register can be as small as two qubits ($n = 2$); however, three qubits ($n = 3$) allow for the possibility of detecting more periods and thus constitutes a more stringent test of the modular exponentiation and QFT [15]. Together with the $m = \lceil \log_2 15 \rceil = 4$ qubits to hold $f(x)$, we need seven qubits in total (Fig. 1b). We implemented this algorithm and tested it on two representative parameter choices: $a = 11$ (an "easy" case) and $a = 7$ (a "difficult" case).

The custom-synthesized molecule used as the quantum computer for this experiment contains five ^{19}F and two ^{13}C spin-1/2 nuclei as qubits (Fig. 2). In a static magnetic field, each spin has two discrete energy eigenstates, $|0\rangle$ (spin-up) and $|1\rangle$ (spin-down), described by the Hamiltonian $\mathcal{H}_0 = -\sum_i \hbar \omega_i I_{zi}$, where $\omega_i/2\pi$ is the transition frequency between $|0\rangle$ and $|1\rangle$ and I_z is the $\hat{z}$ component of the spin angular momentum operator. *All* seven spins in this molecule are remarkably

well separated in frequency $\omega_i/2\pi$, and interact pairwise via the J-coupling, described by $\mathcal{H}_J = \sum_{i<j} 2\pi\hbar J_{ij} I_{zi} I_{zj}$ [17].

The desired initial state of the seven qubits is $|\psi_1\rangle = |0000001\rangle$ (Fig. 1). However, experimentally we start from thermal equilibrium. The density matrix is then given by $\rho_{th} = e^{-\mathcal{H}_0/k_B T}/2^7$, with $k_B T \gg \hbar\omega_i$ at room temperature so each spin is in a statistical mixture of $|0\rangle$ and $|1\rangle$ (Fig. 4a). We converted ρ_{th} into a 7-spin effective pure state [11, 12] ρ_1 via temporal averaging [9] (step 0); ρ_1 constitutes a suitable initial state for Shor's factoring algorithm since it generates the same signal as $|\psi_1\rangle$, up to a proportionality constant [11, 12]. While ρ_1 is highly mixed and in fact remains separable under unitary transforms, the observed dynamics under multiple qubit operations such as in Shor's algorithm apparently remain hard to simulate classically [18, 19, 20].

The quantum circuit of Fig. 1 was realized with a sequence of ~ 300 ($a = 7$) spin-selective radio-frequency (RF) pulses separated by time intervals of free evolution under the Hamiltonian (Fig. 3). The pulse sequence is designed such that the resulting transformations of the spin states correspond to the computational steps in the algorithm. Upon completion of this sequence, we estimate the state of the first three qubits, $\rho \sim \sum_c w_c |c2^3/r\rangle\langle c2^3/r|$, via nuclear magnetic resonance (NMR) spectroscopy. In the experiment, an ensemble of independent quantum computers rather than a single quantum computer was used, so the measurement gives the bitwise average value of $8c/r$, instead of a sample of $8c/r$. This is sufficient to determine r in the present experiment, but for larger N a continued fractions algorithm will need to be performed on the quantum computer [11] requiring additional qubits. From r, at least one factor of N is given by the greatest common denominator (gcd) of $a^{r/2} \pm 1$ and N (with probability greater than $1/2$); the gcd can be computed efficiently using Euclid's algorithm on a classical computer [2] .

The experimental spectra acquired upon completion of the easy case ($a = 11$) of Shor's algorithm (Fig. 4c) clearly indicate that qubits 1 and 2 are in $|0\rangle$ (spectral lines up), and that 3 is in an equal mixture of $|0\rangle$ and $|1\rangle$ (lines up and down, and the integral of the spectrum equal to zero). With qubit 3 the most significant qubit after the inverse QFT [22], the first register is thus in a mixture of $|000\rangle$ and $|100\rangle$, or $|0\rangle$ and $|4\rangle$ in decimal notation. The periodicity in the amplitude of $|y\rangle$

is thus 4, so $r = 2^n/4 = 2$ and we find that $\gcd(11^{2/2} \pm 1, 15) = 3, 5$. The prime factors thus unambiguously derive from the output spectra.

From analogous spectra for the difficult case ($a = 7$; Fig. 4d), we see that qubit 1 is in $|0\rangle$, and qubits 2 and 3 are in a mixture of $|0\rangle$ and $|1\rangle$. The register is thus in a mixture of $|000\rangle$, $|010\rangle$, $|100\rangle$ and $|110\rangle$, or $|0\rangle$, $|2\rangle$, $|4\rangle$ and $|6\rangle$. The periodicity in the amplitude of $|y\rangle$ is now 2, so $r = 8/2 = 4$ and $\gcd(7^{4/2} \pm 1, 15) = 3, 5$. Thus, even after the long and complex pulse sequence of the difficult case, the experimental data conclusively indicate the successful execution of Shor's algorithm to factor 15.

Nevertheless, there are obvious discrepancies between the measured and ideal spectra, most notably for the difficult case. Using a numerical model, we have investigated whether these deviations could be caused by decoherence. A full description of relaxation for the seven coupled spins involves almost $4^7 \times 4^7$ degrees of freedom and requires knowledge of physical properties of the molecule which are not available [23, 24]. In order to get a first estimate of the impact of decoherence during the factoring pulse sequence we assume that each spin experiences independent stochastic relaxation with correlation time scales $\ll 1/\omega_i$. This permits the use of the phenomenological Bloch equations [25], with just two time constants per spin (T_1 and T_2). We implemented this decoherence model for seven coupled spins via the operator sum representation [26] $\rho \mapsto \sum_k E_k \rho E_k^\dagger$ ($\sum_k E_k^\dagger E_k = I$), starting from existing single spin models [27] of generalized amplitude damping (GAD, T_1),

$$E_0 = \sqrt{p} \begin{bmatrix} 1 & 0 \\ 0 & \sqrt{1-\gamma} \end{bmatrix}, \quad E_1 = \sqrt{p} \begin{bmatrix} 0 & \sqrt{\gamma} \\ 0 & 0 \end{bmatrix},$$

$$E_2 = \sqrt{1-p} \begin{bmatrix} \sqrt{1-\gamma} & 0 \\ 0 & 1 \end{bmatrix}, \quad E_3 = \sqrt{1-p} \begin{bmatrix} 0 & 0 \\ \sqrt{\gamma} & 0 \end{bmatrix}. \tag{1}$$

and phase damping (PD, related to T_2),

$$E_0 = \sqrt{\lambda} \begin{bmatrix} 1 & 0 \\ 0 & 1 \end{bmatrix}, \quad E_1 = \sqrt{1-\lambda} \begin{bmatrix} 1 & 0 \\ 0 & -1 \end{bmatrix}, \tag{2}$$

with $\gamma = 1 - e^{-t/T_1}$, $p = 1/2 + \hbar\omega/4k_B T$ and $\lambda \sim (1 + e^{-t/T_2})/2$. The following observations simplify the extension of these separate single spin descriptions to an integrated model for seven

spins: (1) GAD (and PD) error operators acting on different spins commute; (2) the E_k for GAD commute with the E_k for PD when applied to arbitrary ρ; and (3) PD commutes with the ideal unitary time evolution $e^{-i\mathcal{H}t}$ ($\mathcal{H} = \mathcal{H}_0 + \mathcal{H}_J$). However, GAD does *not* commute with $e^{-i\mathcal{H}t}$, and PD and GAD do *not* commute with the ideal unitary evolution during RF pulses. Nevertheless, we have treated these as commuting transformations, such that all of the processes which occur simultaneously can be modeled sequentially.

Specifically, the model simulates a delay time of duration t_d by $e^{-i\mathcal{H}t_d}$ followed by GAD acting on spin 1 for a duration t_d, then GAD acting on spin 2 and so forth, followed by PD acting serially on each spin. Similarly, a shaped pulse of duration t_p was modeled by a delay time of duration t_p ($e^{-i\mathcal{H}_0 t_p}$, GAD and PD) followed by an instantaneous pulse. Using this simple model, the 7-spin simulation of the complete Shor pulse sequence, including 36 temporal averaging sequences, required only a few minutes on an IBM quad POWER3-II processor machine. Measured values of T_1 and T_2 (Fig. 2) were used in the model.

The output spectra predicted by this parameter-free decoherence model are also shown in Figs. 4c and d. While some discrepancies between the data and the simulations remain (due to the approximations in the model as well as due to experimental imperfections such as RF inhomogeneity, imperfect calibrations, incomplete field drift compensation and incomplete unwinding of coupled evolution during the RF pulses [15]), the model agrees well with the large non-idealities of the data. The predictive value of the model was further confirmed via independent test experiments.

This is the first NMR quantum computation experiment for which decoherence is the dominant source of errors [8]; the demands of Shor's algorithm clearly push the limits of the current molecule, despite its exceptional properties. At the same time, the good agreement between the measured and simulated spectra suggests that the degree of unitary control in the experiment was very high, which bodes well for related proposed implementations of quantum computers [28, 29]. Finally, our parameter-free decoherence model, a predictive tool for modeling quantum errors in this complex

system, provides an avenue for future design simulation of quantum computers.

Methods

Experiments were performed at the IBM Almaden Research Center with an 11.7 T (500 MHz) Oxford Instruments magnet, a custom-modified four-channel Varian Unity INOVA spectrometer, and a Nalorac HFX probe. We extended the techniques of Ref. [9] for serving multiple nuclei per channel, for reducing cross-talk between RF pulses on different spins and for sending simultaneous pulses. We used spin-selective Hermite-180 and Gaussian-90 pulses [17], shaped in 256 steps, with a duration of 0.22 to ~ 2 ms. A technique to compensate for coupling effects during the selective pulses was developed and implemented via "negative delay" times before *and* after the pulse. The amount of negative evolution needed depends on the pulse shape and was pre-computed via numerical simulations.

To create an effective pure ground state of *all seven* spins, which has never been done before, we used a two-stage extension of the scheme of Ref. [9], necessary because $\omega_{^{13}C}$ is very different from $\omega_{^{19}F}$. The five ^{19}F spins are made effective pure via the summation of nine experiments, each with a different sequence of CN_{ij} and N_i gates (CN_{ij} stands for a controlled-NOT operation, which flips the target qubit j if and only if the control i is in $|1\rangle$; N_i simply flips i) [27]. These nine experiments are executed four times, each time with different additional CN_{ij} and N_i, such that the two ^{13}C spins are also made effective pure. Summation of the $4 \times 9 = 36$ experiments along with a NOT on spin 7 gives ρ_1. The state preparation sequences were designed to be as short as possible (~ 200 ms) by making optimal use of the available coupling network [15].

Multiplication of $y = 1$ by $a \bmod 15$ controlled by x_0 (qubit 3) was replaced by controlled-addition of $(a - 1) \bmod 15$. For $a = 11$, this is done by $CN_{34}CN_{36}$ and for $a = 7$ by $CN_{35}CN_{36}$ (gates A and B of Fig. 1b). Multiplication of y by $7^2 \bmod 15$ is equivalent to multiplication of y by 4 mod 15, which reduces to swapping y_0 with y_2 and y_1 with y_3. Both SWAP operations must be controlled by x_1, which can be achieved [30] via gates C, D, E and F, G, H of Fig. 1b. This quantum circuit can be further simplified by a quantum analogue to peephole compiler opti-

mization [31], which should become standard in future quantum compilers: (1) the control qubit of gate C is $|0\rangle$, so C was suppressed; (2) similarly, F was replaced by N_5; (3) gates H and E are inconsequential for the final state of the first register, so they were omitted; (4) the targets of the doubly controlled NOT gates D and G are in a basis state, so they can be implemented as $CY_{24}^\dagger CZ_{64}^2 CY_{24}$ and $CY_{27}^\dagger CZ_{57}^2 CY_{27}$ (CZ_{ij} stands for a $90°$ $\hat{z}$ rotation of j if and only if i is in $|1\rangle$); (5) the refocusing schemes were kept as simple as possible. To this end, A was carried out after E. We did refocus inhomogeneous dephasing for all spins in the transverse plane. Residual couplings with the cyclopentadienyl protons were decoupled by continuous on-resonance low power irradiation using a separate power amplifier and additional power combiners and RF filters. After all these simplifications, the pulse sequence for 7^x mod 15 was ~ 400 ms long. The inverse QFT was implemented as shown in Fig. 1b and took ~ 120 ms. The duration of the complete sequence for the Shor algorithm was thus up to ~ 720 ms. A detailed report on these methods will be published elsewhere [15].

REFERENCES

[1] Knuth, D.E. *The Art of Computer Programming, Vol. 2: Seminumerical Algorithms* (Addison-Wesley, Reading, Mass., 1998).

[2] Koblitz, N. *A Course in Number Theory and Cryptography* (Springer-Verlag, New York, 1994).

[3] Bennett, C.H. & DiVincenzo, D.P. Quantum information and computation. *Nature* **404**, 247–255 (2000).

[4] Shor, P. Algorithms for quantum computation: discrete logarithms and factoring. *Proc. 35th Ann. Symp. on Found. of Comp. Sci.*, 124–134 (IEEE Comp. Soc. Press, Los Alamitos, CA, 1994).

[5] Shor, P. Polynomial-time algorithms for prime factorization and discrete logarithms on a quantum computer. *SIAM J. Computing*, **26**, 1484–1509 (1997)

[6] Ekert, A. & Jozsa, R. Quantum computation and Shor's factoring algorithm. *Rev. of Mod.*

Phys. **68**, 3, 733–753 (1996).

[7] Beckman, D., Chari, A.N., Devabhaktuni S. & Preskill, J. Efficient networks for quantum factoring. *Phys. Rev. A* **54**, 1034 (1996).

[8] Jones, J.A. NMR quantum computation. *Progr. NMR Spectr.*, **38**, 325–360 (2001).

[9] Vandersypen, L.M.K., *et al.* Experimental realization of an order-finding algorithm with an NMR quantum computer. *Phys. Rev. Lett.* **85**, 5452–5455 (2000).

[10] Knill, E., Laflamme, R., Martinez, R. & Tseng, C.-H. An algorithmic benchmark for quantum information processing. *Nature* **404**, 368–370 (2000).

[11] Gershenfeld N. & Chuang, I.L. Bulk spin-resonance quantum computation. *Science* **275**, 350–356 (1997).

[12] Cory, D.G., Fahmy, A.F. & Havel, T.F. Ensemble quantum computing by NMR spectroscopy. *Proc. Nat. Acad. Sci.* **94**, 1634–1639 (1997).

[13] Schulman, L. & Vazirani, U. Molecular Scale Heat Engines and Scalable NMR Quantum Computation. *Proceedings of the 31st ACM Symposium on Theory of Computing* 322–329 (1999).

[14] Chuang, I.L., Laflamme, R., Shor, P. & Zurek, W.H. Quantum Computers, Factoring, and Decoherence. *Science* **270**, 1633 (1995).

[15] Steffen, *et al. in preparation.*

[16] Green, M., Mayne, N. & Stone, F.G.A. Chemistry of the metal carbonyls. Part XLVI. Perfluorobutadienyl iron, rhenium and manganese complexes. *J. Chem. Soc. (A)*, 902–905 (1968).

[17] Freeman, R. *Spin Choreography* (Spektrum, Oxford, 1997).

[18] Braunstein, S. L. et al. Separability of very noisy mixed states and implications for NMR quantum computing. *Phys. Rev. Lett.* **83**, 1054–1057 (1999);

[19] Schack, R. and Caves, C. M. Classical model for bulk-ensemble NMR quantum computation. *Phys. Rev. A* **60**, 4354–4362 (1999).

[20] Linden, N. & Popescu, S. Good Dynamics versus Bad Kinematics: Is Entanglement Needed for Quantum Computation? *Phys. Rev. Lett.* **87**, 047901 2001

[21] Leung, D. W., *et. al.* Efficient implementation of selective recoupling in heteronuclear spin systems using Hadamard matrices. *Phys. Rev. A* **61**, 0423101–7.

[22] Coppersmith, D. An approximate Fourier transform useful in quantum factoring. *IBM Res. Rep. RC19642* (1994).

[23] Vold, R.L. & Vold, R.R. Nuclear magnetic relaxation in coupled spin systems. *Progr. in NMR Spectr.* **12**, 79–133 (1978).

[24] Jeener, J. Superoperators in magnetic resonance. *Adv. Magn. Res.* **10**, 1–51 (1982).

[25] Bloch, F. Nuclear induction. *Phys. Rev.* **70**, 460–474 (1946).

[26] Kraus, K. *States, Effects, and Operations: Fundamental Notions of Quantum Theory.* (Springer-Verlag, Berlin, 1983).

[27] M.A. Nielsen & I.L. Chuang. *Quantum computation and quantum information.* (Cambridge Univ. Press, Cambridge, England, 2000).

[28] Kane, B.E. A silicon-based nuclear spin quantum computer. *Nature* **393**, 133–137 (1998).

[29] Loss, D. & DiVincenzo, D.P. Quantum computation with quantum dots. *Phys. Rev. A* **57**, 120–126 (1998).

[30] Vandersypen, L.M.K., *et al.* Implementation of a three-quantum-bit search algorithm. *Appl. Phys. Lett.* **76**, 646–648 (2000).

[31] Aho, A.V., Sethi R, & Ullman J.D. *Compilers: Principles, Techniques and Tools* (Addison-Wesley, 1986).

Acknowledgements

Correspondence and requests for materials should be addressed to ILC (e-mail: ichuang@media.mit.edu).

FIG. 1 a. Outline of the quantum circuit for Shor's algorithm. Wires represent qubits and boxes represent operations. Time goes from left to right. **(0)** Initialize a first register of $n = 2\lceil \log_2 N \rceil$ qubits to $|0\rangle \otimes \ldots \otimes |0\rangle$ (for short $|0\rangle$) and a second register of $m = \lceil \log_2 N \rceil$ qubits to $|0\rangle \otimes \ldots \otimes |0\rangle \otimes |1\rangle$ ($|1\rangle$). **(1)** Apply a Hadamard transform H to the first n qubits, so the first register reaches $\sum_{x=0}^{2^n-1} |x\rangle / \sqrt{2^n}$. **(2)** Multiply the second register by $f(x) = a^x \bmod N$ (for some random $a < N$ which has no common factors with N), to get $|\psi_2\rangle = \sum_{x=0}^{2^n-1} |x\rangle |1 \times a^x \bmod N\rangle / \sqrt{2^n}$. Since the first register is in a superposition of 2^n terms $|x\rangle$, the modular exponentiation is computed for 2^n values of x in parallel. **(3)** Perform the inverse QFT on the first register [22], giving $|\psi_3\rangle = \sum_{y=0}^{2^n-1} \sum_{x=0}^{2^n-1} e^{2\pi i x y / 2^n} |y\rangle |a^x \bmod N\rangle / 2^n$, where interference causes only terms $|y\rangle$ with $y = c2^n/r$ (for integer c) to have a substantial amplitude, with r the period of $f(x)$. **(4)** Measure the qubits in the first register. On an ideal single quantum computer, the measurement outcome is $c2^n/r$ for some c with high probability, and r can be quickly deduced from $c2^n/r$ on a classical computer via continued fractions [2]. **b.** Detailed quantum circuit for the case $N = 15$ and $a = 7$. Control qubits are marked by $\bullet$; $\oplus$ represents a NOT operation and 90 and 45 represent $\hat{z}$ rotations over these angles. The gates shown in dotted lines can be removed by optimization and the gates shown in dashed lines can be replaced by simpler gates (see the methods section).

FIG. 2 Structure and properties of the quantum computer molecule, a perfluorobutadienyl iron complex with the inner two carbons ^{13}C-labeled. Based on the measured $J_{^{13}\mathrm{C}^{19}\mathrm{F}}$ values, we concluded that the placement of the iron is as shown, different than derived in Ref.[16] from infrared spectroscopy. The table gives the $\omega_i/2\pi$ at 11.7 T, relative to a reference frequency of ~ 470 MHz and ~ 125 MHz for ^{19}F and ^{13}C respectively [Hz], the longitudinal (T_1, inversion recovery) and transverse (T_2, estimated from a single spin-echo sequence) relaxation time constants [s], and the J-couplings [Hz]. Ethyl (2-^{13}C)bromoacetate (Cambridge Isotope Laboratories, Inc.) was converted to ethyl 2-fluoroacetate by heating with AgF followed by hydrolysis to sodium fluoroacetate using NaOH in MeOH. This salt was converted to 1,1,1,2-tetrafluoroethane using MoF$_6$ and was subsequently treated with two equivalents of BuLi followed by I$_2$ to provide trifluoroiodoethene. Half of the ethene was converted to the zinc salt which was recombined with the remaining ethene and coupled using Pd(Ph$_3$P)$_4$ to give (2,3-^{13}C)hexafluorobutadiene. The end product was obtained by reacting this butadiene with the anion obtained from treating [(π-C$_5$H$_5$)Fe(CO)$_2$]$_2$ with sodium amalgam [16]. The product was purified with column chromatography, giving a total yield of about 5%. The sample at 0.88 ± 0.04 mole $\%$ in diethyl ether-d10 was dried using 3 Å molecular sieves, filtered through a 0.45 μm syringe filter and flame sealed in the NMR sample tube using three freeze-thaw vacuum degassing cycles. All experiments were performed at $30°$C.

FIG. 3 Pulse sequence for implementation of the quantum circuit of Fig. 1 for $a = 7$. The tall red lines represent $90°$ pulses selectively acting on one of the seven qubits (horizontal lines) about positive $\hat{x}$ (no cross), negative $\hat{x}$ (lower cross) and positive $\hat{y}$ (top cross). Note how single $90°$ pulses correspond to Hadamard gates and pairs of such pulses separated by delay times correspond to two-qubit gates. The smaller blue lines denote $180°$ selective pulses used for refocusing [21], about positive (darker shade) and negative $\hat{x}$ (lighter shade). Rotations about $\hat{z}$ are denoted by smaller and thicker green rectangles and were implemented with frame-rotations. Time delays are not drawn to scale. The vertical dashed black lines visually separate the steps of the algorithm; step (0) shows one of the 36 temporal averaging sequences.

FIG. 4 NMR spectra at different stages in the computation. **a.** Experimentally measured thermal equilibrium spectra (real part), acquired after a read-out pulse on spin i has tipped the spin from $|0\rangle$ $(+\hat{z})$ or $|1\rangle$ $(-\hat{z})$ into the $\hat{x} - \hat{y}$-plane, where it induces a voltage oscillating at $\omega_i/2\pi + \sum_j \pm J_{ij}/2$ (where the sign depends on the state of the other spins) in a transverse RF coil placed nearby the sample. This voltage was recorded by a phase-sensitive detector and Fourier transformed to obtain a spectrum, with the phase set such that positive (negative) lines correspond to a spin in $|0\rangle$ $(|1\rangle)$ before the readout pulse. Frequencies are in Hertz, and with respect to $\omega_i/2\pi$. **b.** Experimental spectra for the effective pure ground state. As desired, only one line is retained in each multiplet with its position depending on strength and sign of the J-couplings. Here, the transition corresponds to all other spins in $|0\rangle$. The state ρ_1 is obtained from this state by applying a NOT on spin 7. **c.** Output spectra of the easy case of Shor's algorithm $(a = 11)$. The top traces are the ideally expected spectra, the middle traces are the experimental data, and the bottom traces are simulations which incorporate decoherence effects (vide infra). Each trace was rescaled separately. **d.** Similar set of spectra as in c, but for the difficult case $(a = 7)$.
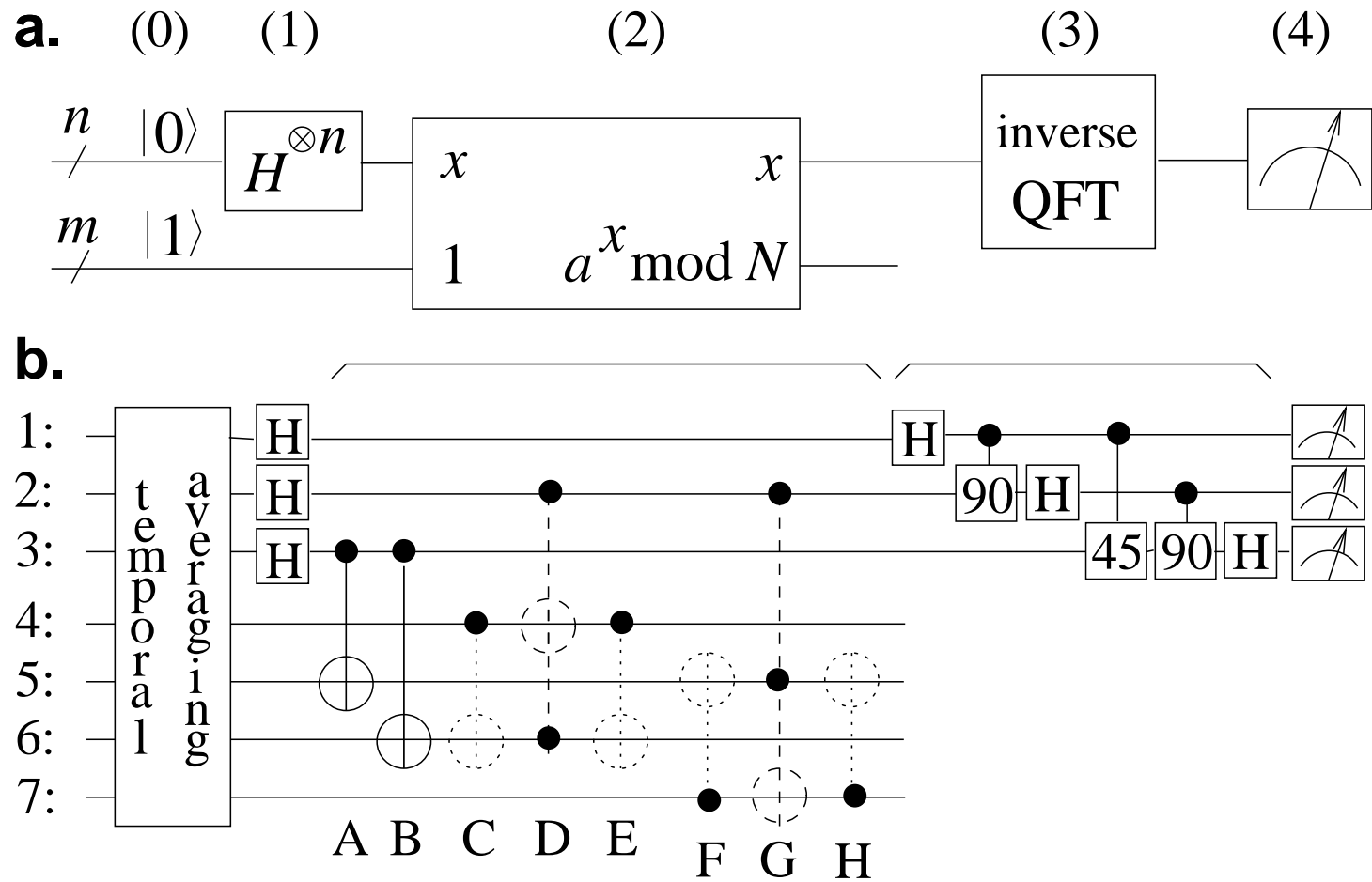
Figure 1

L. Vandersypen NATURE 07-Sep-01

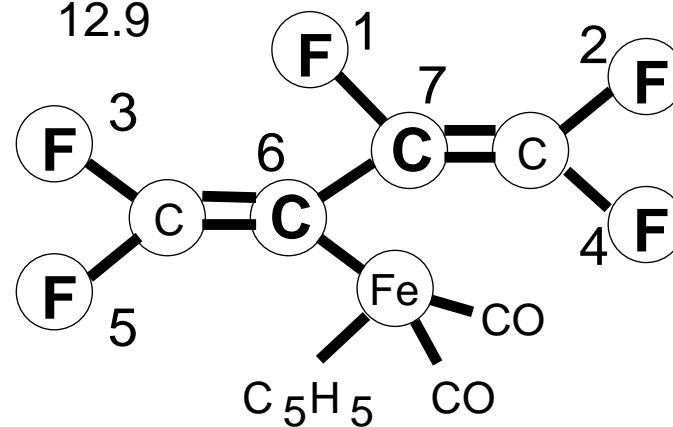| i	$\omega_i / 2\pi$	$T_{1,i}$	$T_{2,i}$	J_{7i}	J_{6i}	J_{5i}	J_{4i}	J_{3i}	J_{2i}
1	−22052.0	5.0	1.3	−221.0	37.7	6.6	−114.3	14.5	25.16
2	489.5	13.7	1.8	18.6	−3.9	2.5	79.9	3.9	
3	25088.3	3.0	2.5	1.0	−13.5	41.6	12.9		
4	−4918.7	10.0	1.7	54.1	−5.7	2.1			
5	15186.6	2.8	1.8	19.4	59.5				
6	−4519.1	45.4	2.0	68.9					
7	4244.3	31.6	2.0						

Figure 2
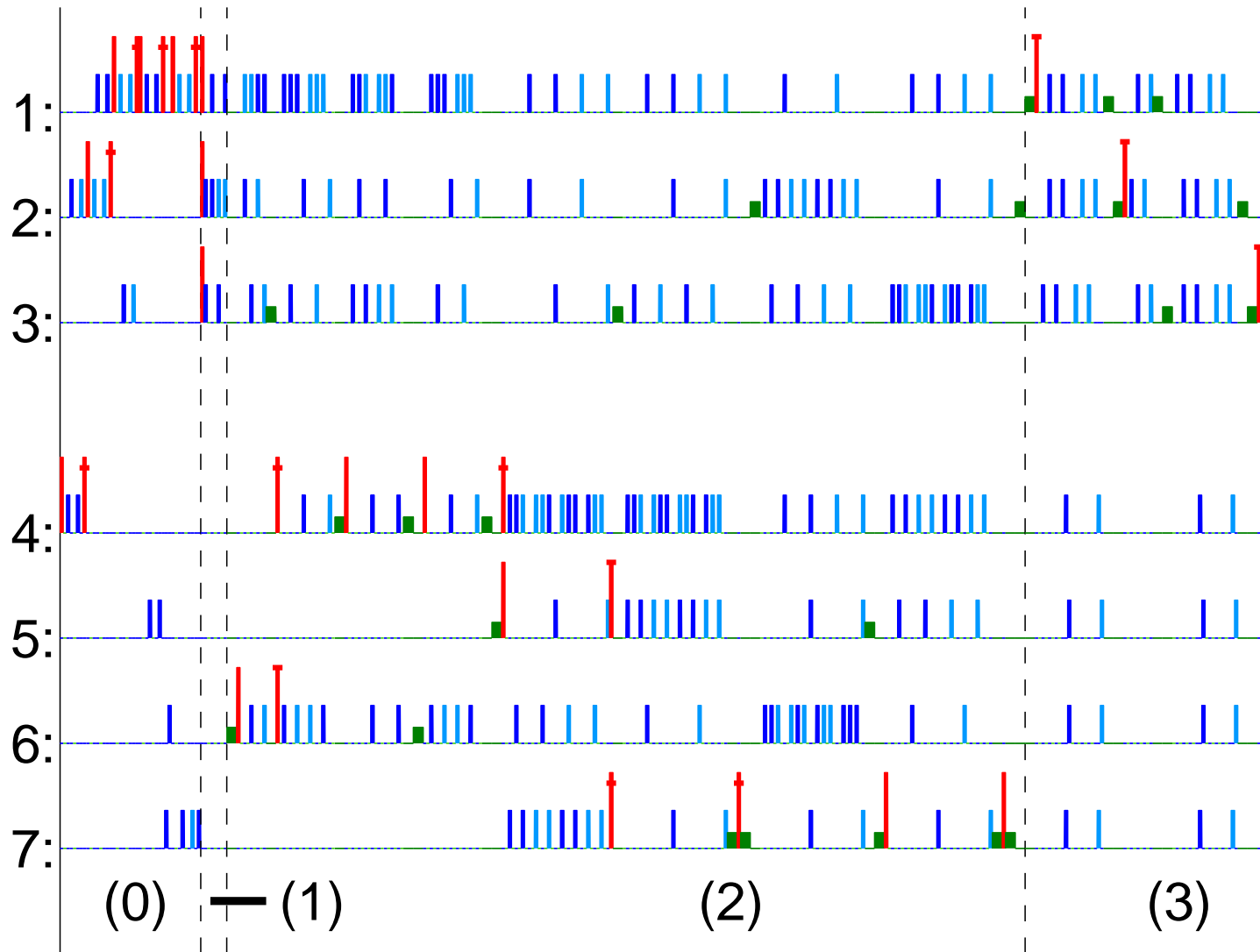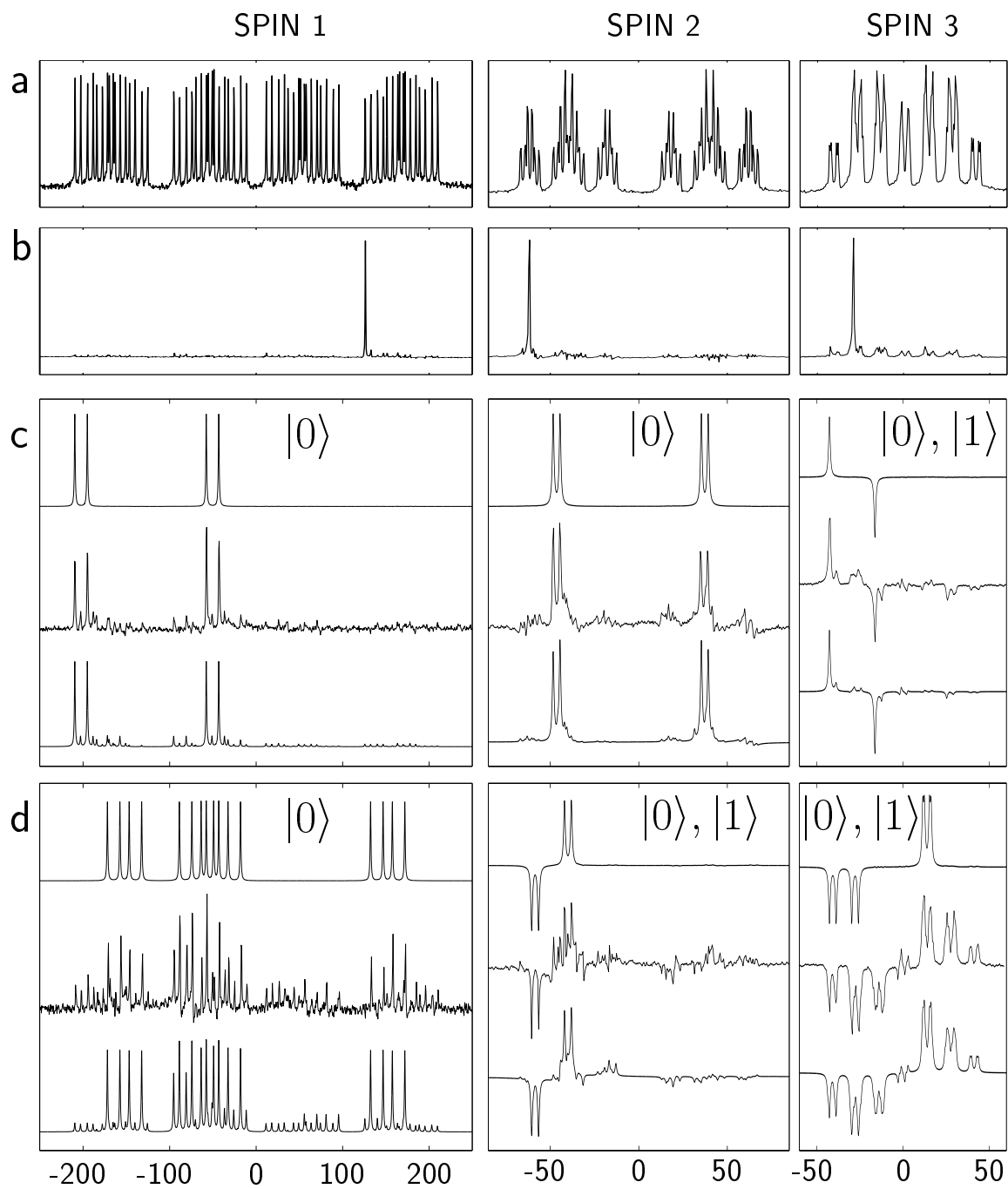
L. Vandersypen NATURE 07-Sep-01

Figure 3

L. Vandersypen NATURE 07-Sep-01

Figure 4

L. Vandersypen NATURE 07-Sep-01